Proceedings of the ASME 2010 3rd Joint US-European Fluids Engineering Summer Meeting and 8th International Conference on Nanochannels, Microchannels, and Minichannels
FEDSM-ICNMM2010
August 1-5, 2010, Montreal, Canada

FEDSM-ICNMM2010-30674

A CHARACTERIZATION OF LIMIT CYCLE OSCILLATIONS IN MEMBRANE WING MICRO AIR VEHICLES AT LOW ANGLE OF ATTACK

Peter J. Attar
School of Aerospace and Mechanical Engineering
The University of Oklahoma
Norman, Oklahoma, 73071
e-mail: peter.attar@ou.edu

Jordan W. Johnston, **William A. Romberg**, **Ramkumar N. Parthasarathy**, **Brian J. Morris**
School of Aerospace and Mechanical Engineering
The University of Oklahoma
Norman, Oklahoma, 73071

ABSTRACT

In this paper, a (three) batten-reinforced fixed wing membrane micro air vehicle is used to determine the effect of membrane pre-strain on flutter and limit cycle behavior of fixed wing membrane Micro Air Vehicles. For each configuration tested, flutter and subsequent limit cycle oscillations are measured in wind tunnel tests and predicted using an aeroelastic computational model consisting of a nonlinear finite element model coupled to a vortex lattice solution of the Laplace equation and boundary conditions. Agreement between the predicted and measured onset of limit cycle oscillation is good as is the prediction of the amplitude of the limit cycle at the trailing edge of the lower membrane. A direct correlation between levels of strain and the phase of the membranes during the limit cycle is found in the computation and thought to also occur in the experiment.

Introduction

The use of small unmanned vehicles, often called Micro Air Vehicles (MAVs), offers many benefits in the areas of civilian and military surveillance. Often consisting of wing spans which measure less than 6 inches, these vehicles are readily deployable and leave minimal acoustic footprint and are able to enter dangerous environments potentially placing less risk on human life. Currently three separate classes of MAVs exist; fixed wing vehicles; rotary wing vehicles; and flapping wing configurations. Each of these has its own unique set of benefits and pitfalls. In the work to be presented in this two part investigation, simplified fixed wing and flapping wing models will be analyzed in an attempt to better understand the complex physics involved in the flight of these vehicles in order to aid in improved design and control.

The addition of flexibility to lifting surfaces, whether they are flapping or fixed, would appear to have many potential benefits. The simplest of these is the weight reduction possible if flexibility is allowed. Achieving adequate propulsion for MAVs remains a key issue therefore any reduction in weight will be of great benefit. Second, the addition of flexibility has the potential to improve aerodynamic performance. For example, in studies performed by Heathcote et al. [1] and Heathcote and Gursul [2], the introduction of a moderate level of chordwise and spanwise flexibility was found to be beneficial for heaving airfoils. Also work by Shyy and his colleagues on the aerodynamic performance of batten-stiffened fixed-wing membrane MAVs (MMAVs) [3–8] has shown that the flexibility in these wings leads to better stall characteristics for a given airfoil shape and improved controllability due to their ability to more easily absorb energy from atmospheric gusts.

On the other hand, the intentional introduction of flexibility into lifting surfaces brings with it the potential problem of increased risk of detrimental aeroelastic phenomenal such as static divergence, flutter and buffet. Previous work by Hu et al. [9] have reported encountering, at low angle of attack, what appears to be stable limit cycle but no comprehensive study has been conducted to thoroughly investigate this. Hence in this paper we will examine, through computation and experiment, the aeroelastic behavior of a simplified three batten MMAV for various levels of membrane pre-strain and small fixed angle of attack.

Experimental and Computational Models

The three batten wind tunnel model is shown in Fig. 1. In this figure the leading edge is to the right of the model (i.e. flow is right to left). The chord and span dimensions are 11.43 cm and 15.24 cm respectively and the battens have a spanwise dimension of 0.64 cm. The model is mounted vertically in the wind tunnel. The experiments are performed in the University of Oklahoma low speed, open loop wind tunnel. This tunnel contains a circular test section of inner diameter 45.72 cm and length 76.2 cm and is capable of producing flow between 1.5 and 34 m/s. In order to measure peak deflections, a high speed camera is used along with a reference scale at the base of the model. Strain measurements are taken at a location 3.05 cm from the root and 0.32 cm. from the leading edge. The model frames are constructed of 1.59 mm aluminum over which 0.15 mm latex rubber material is stretched to a given level of pre-strain. The latex is adhered to the aluminum frame using a trim adhesive. Pre-strain measurements were taken at a number of locations on the wing surface and minimal differences were noted. The estimated accuracy of the applied pre-strain on any MMAV is $\pm 0.2\%$. For more details on the experimental model and setup please see Ref. [10].

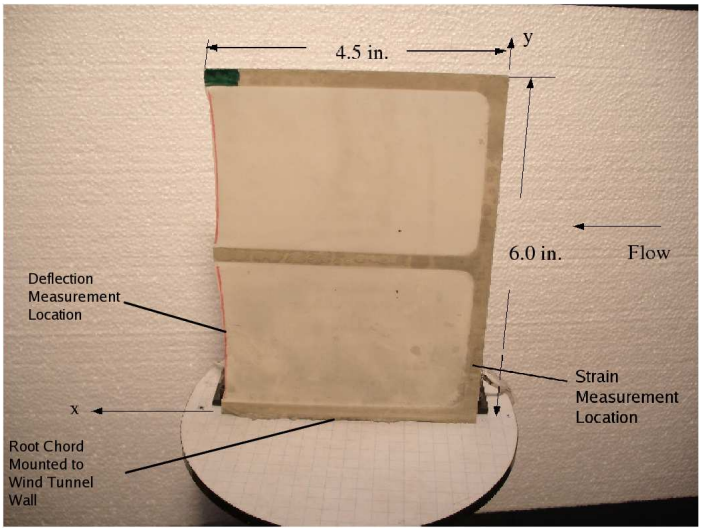

Figure 1. Photograph of three batten experimental model.

Membrane and batten deformation data are collected through the use of a MotionProX3 high speed camera utilizing a 25mm Fujinon lens connected to a dedicated Sony Vaio laptop. Resolution is set so that a single pixel measures .0178 cm wide; this is to ensure that the focus remains constant and repeatable between tests. The camera is mounted directly above the model on the outer wall of the test section, and recorded at 1250 fps. Two 250 Watt halogen lamps provide lighting of the model. Image analysis is carried out using the software MotionPro Studio; deformations are calculated based upon image pixel width and a reference scale built in to the specimen's mounting fixture. Recordings are taken at flow velocities ranging from 1.5 to 8.5 m/s in increments of .5 m/s. In order to quantify uncertainty, six recordings were taken of a given batten/prestrain configuration at a single flow velocity in the post flutter regime. Ten latex deflection measurements were recorded for each video recording. The uncertainty analysis was performed as described in Ref. 11, and the uncertainty in the measurement of the deflection of the latex membrane wing skin was found to be ± 0.032 cm with 95% confidence.

The computational model consists of a nonlinear structural dynamics finite element model coupled to a vortex lattice model for the aerodynamics. The finite element model utilizes plate elements derived using the GL3 formulation described in Ref. [12] with different material and thickness properties given to the elements which correspond to the latex and aluminum materials. The mesh used in the structural dynamic computations, which consists of 1287 quadrilateral elements, is shown in Fig. 2. The computational model boundary conditions are fully clamped for the complete root chord. Linear elastic material properties are assumed for both the batten (aluminum) and membrane (latex) material.

The vortex lattice aerodynamic model uses linearized, small perturbation boundary conditions and a planar wake is assumed. On the wing, 50 and 40 ring vortices are used in the spanwise chordwise directions respectively. The number of wake elements kept is such that for a given flow velocity and timestep, at least 3 chords of wake are considered. A symmetry boundary condition is imposed in order to account for the effect of the wind tunnel wall. See Ref. [13] for more details on the vortex lattice solution for unsteady potential flow problems.

As the structural dynamic nodes and aerodynamic collocation points do not coincide, a local bilinear interpolation of forces,displacements and velocities is used to transfer these quantities between the two mesh domains. This interpolation is force conserving as finite element shape functions are used. See Ref. [14] for more details on this interpolation.

Since the fluid and structural equations are solved separately,

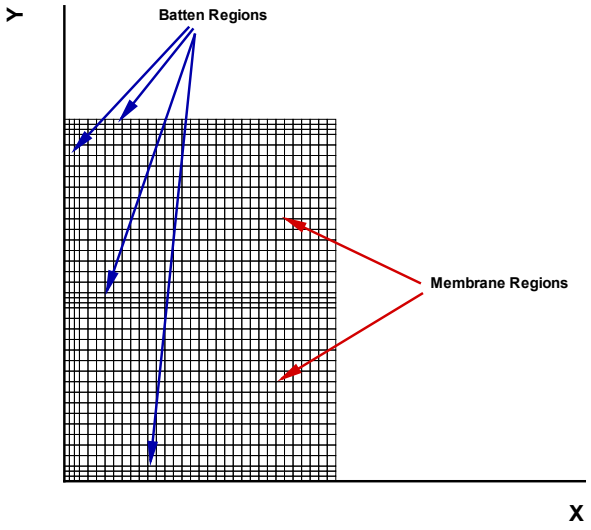

Figure 2. Computational mesh used for structural dynamics.

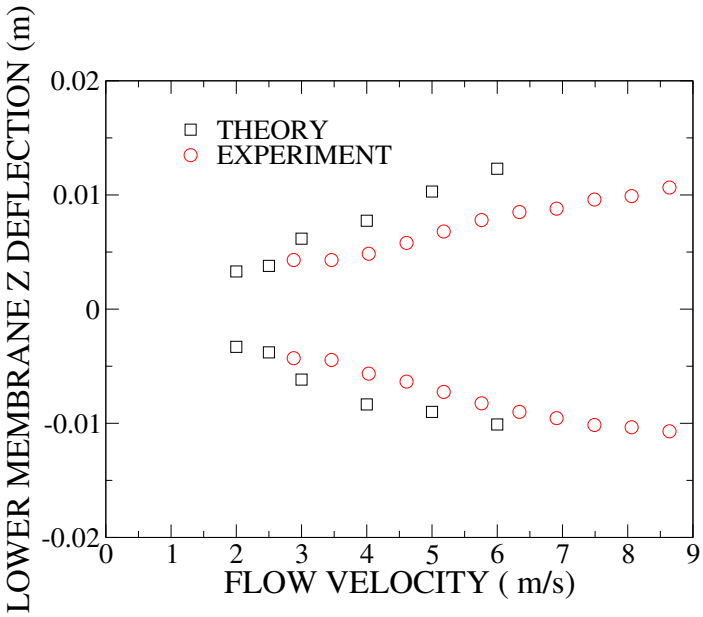

Figure 3. Deflection of MMAV versus flow velocity for 2 percent pre-strain model at 0 degree angle of attack.

subiteration is performed within a timestep in order to ensure that errors do not occur due to the introduction of a time lag in the solution. A subiteration convergence criteria of 1.0e-4 is used for L2 norm of the fluid circulation (field variables in vortex lattice model) and structural displacements and velocities.

Batten Stiffened Membrane Micro Air Vehicle

Experimental and computational results will be presented for a 3 batten configuration with various levels of pre-strain (2,5,7 and 10 percent). Also experiments have been performed at three static angles of attack, 0,1 and 2 degrees. For all but one configuration, the results are quite insensitive to the angle attack for these low angles of attack. Therefore, for all but the aforementioned case of interest which displays some sensitivity to this parameter, results will only be presented at 0 angle of attack. The range of flow velocities studied results in Reynolds numbers which range from a minimum of 1.5×10^4 to a maximum of 1.3×10^5.

The first configuration to be discussed is the 2 percent pre-strain model at zero degree angle of attack. Shown in Fig. 3 is the membrane deflection, measured at the midpoint of the lower membrane (see Fig. 7) at the trailing edge versus the flow velocity. For flow velocities below the first reported data point, both the computation and experiment (to within the accuracy of the deflection measurement) had zero deflection. This is true for all figures in this paper which report deflection versus flow velocity. In the computational model, the flow velocity where the model undergoes a Hopf bifurcation (self-excited instability) also known as the flutter point, is approximately 1.75 m/s while the experimental results show a dramatic increase in membrane deflection (indicating instability) near 3 m/s. After the Hopf bifurcation occurs, and this is the case in the experiment and computation for each model tested, stable limit cycle oscillations (LCOs) exist. As the only nonlinearity which is included in the computational aeroelastic model is due to the structural model, these limit cycles (at least the computationally predicted ones) are caused by the geometric nonlinearity in the structure. In both the experiment and computations, the nonlinearity appears to be quite strong signified by the slow increase in LCO response amplitude with an increase in the bifurcation parameter (flow velocity).

Shown in Figs. 4 and 5 is the root-mean square (RMS) of the y normal strain (ε_{yy}) and dominant LCO frequency versus flow velocity. The computational strain results appear to have three levels of response, two large and one small, while the experimental model seems to contain two levels. In the experiment, three levels of frequencies are noted, the last jump occurring where the strain jump occurs in Fig. 4 ($\approx$ 6 m/s). Similar to the experimental model, the frequency of LCO increases with flow velocity in the computations. Unlike the experimental results, this increase appears to be smooth. It is also found that for this level of pre-strain, the frequency content of the experimental response consists of two very close frequencies. The result of this is a strain time history which is modulated ("beating"), as shown in Fig. 6

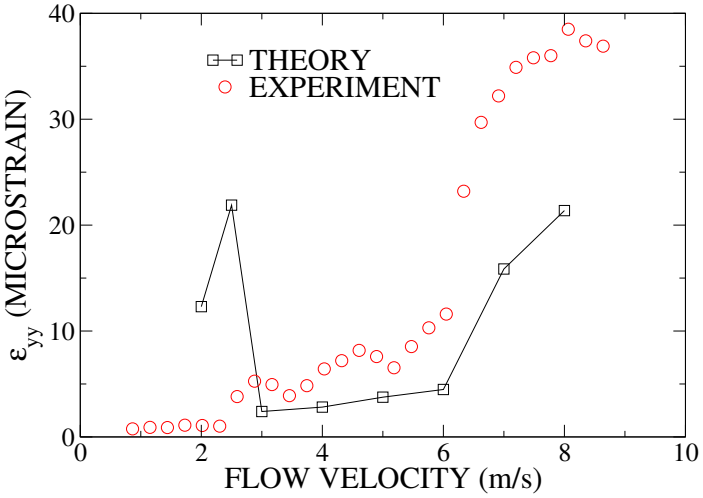

Figure 4. Root mean square of MMAV y normal strain versus flow velocity for 2 percent pre-strain model at 0 degree angle of attack.

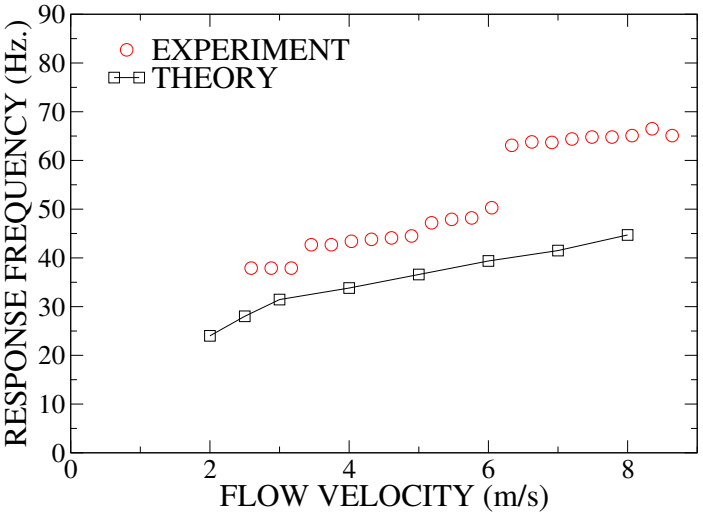

Figure 5. Dominant MMAV structural response frequency versus flow velocity for 2 percent pre-strain model at 0 degree angle of attack.

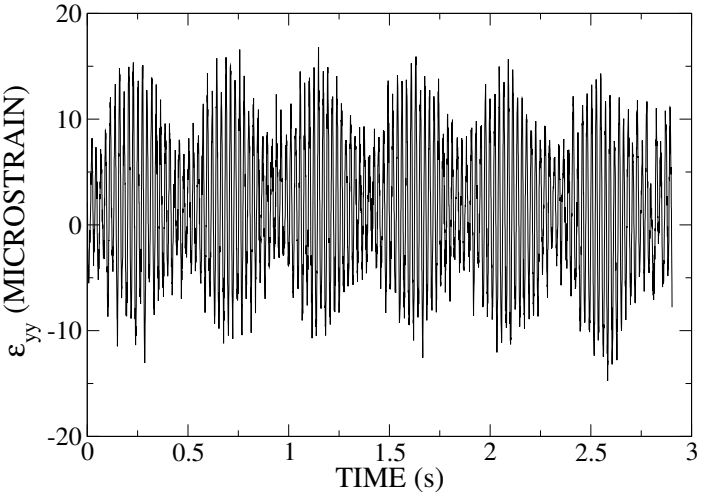

Figure 6. Experimentally measured response of y normal strain versus time for 2 percent pre-strain model at 0 degree angle of attack and 4.0 m/s

For the computational model, and it is postulated, for the experimental model, the different strain levels in Fig. 4 can be explained by a switch in mode of oscillation. In the computation it is found that when the LCO occurs such that the trailing edge upper and lower membranes oscillate in phase, a large amplitude strain branch occurs while if they are oscillating out-of-phase, a lower amplitude branch occurs. This is demonstrated by comparing the response levels in Fig. 4 to the three figures which display the LCO mode of oscillation at three different flow velocities, Figs. 7-9. In Figs. 7 and 9, which correspond to flow velocities of 2 and 8 m/s, it can be seen that the LCO response is such that the two membranes are oscillating in phase and the resulting strain level in Fig. 4 is high. In Fig. 8, the response is out-of-phase and the resulting strain level in Fig. 4 is low. This strong dependence of strain response on the phase of the membranes is also seen for other levels of pre-strain as will be shown later in this section. It should also be obvious that this behavior of the strain response is a function of the location of measurement. Although not investigated, there are surely locations which will experience increased strain levels when the membranes switch to out-of-phase behavior.

Also, it is evident that while the strain response is sensitive to the mode of vibration, a switch in the response does not appear to effect the magnitude of the trailing edge membrane deflection. This is clearly shown in Fig. 3 where the membrane deflection appears to vary smoothly with flow velocity in both the experiment and computation.

It should also be noted that while the computational and experimental strain values both appear to have a dramatic increase near 6 m/s only the experimental values show a jump in the frequency of the response at this flow velocity. While the computational model switches mode of oscillation at this flow velocity, this switch does not cause any apparent jump in frequency. Instead, the response seems to smoothly vary from what appears to be a coupling of structural dynamic modes 5 and 6 at a flow velocity of 2 m/s to one which is a coupling of structural dynamic modes 2 and 3 for a flow velocity of 6 m/s and then finally show-

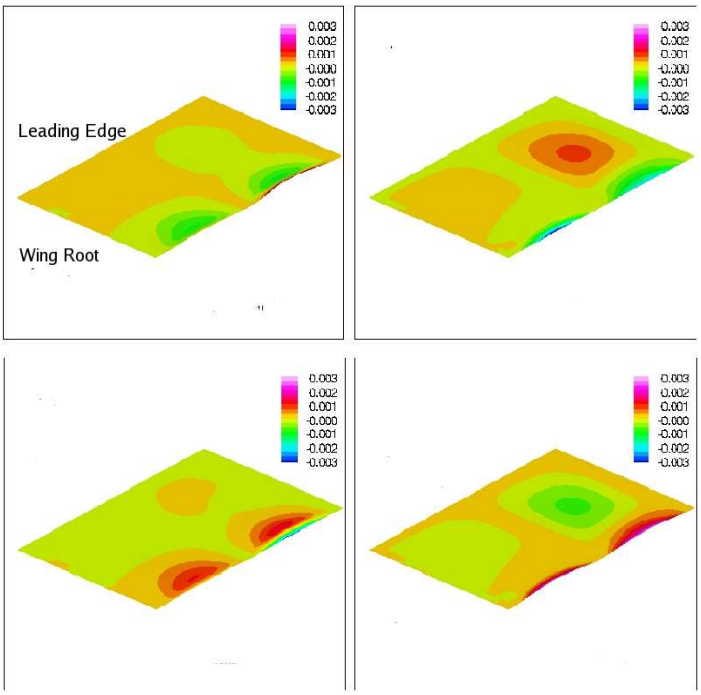

Figure 7. Computed spatial configuration (mode) of MMAV at 4 points in time during the limit cycle period for 2 percent pre-strain model at 0 degree angle of attack at 2.0 m/s

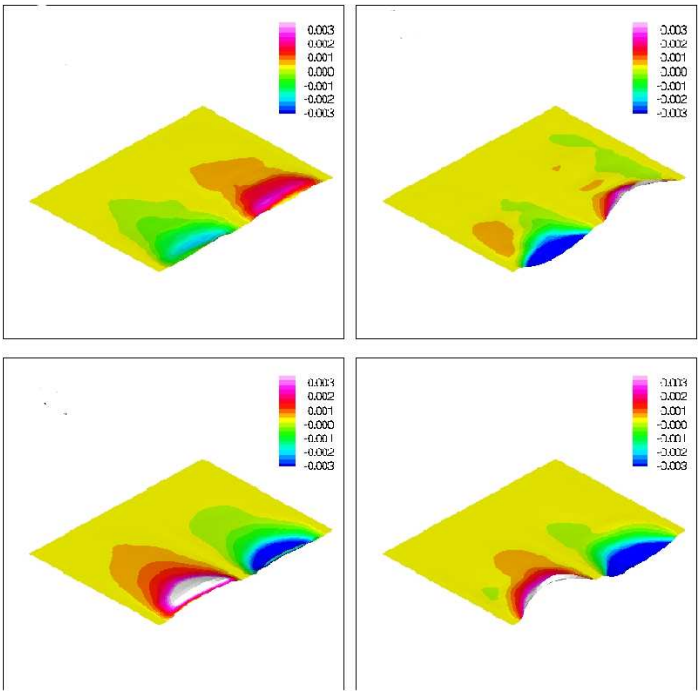

Figure 8. Computed spatial configuration (mode) of MMAV at 4 points in time during the limit cycle period for 2 percent pre-strain model at 0 degree angle of attack at 6.0 m/s

ing a response which appears to couple modes 13 and 14 for a flow velocity of 8 m/s. These linear structural dynamic modes, generated using the commercial software package ANSYS [15] and computed about an undeformed configuration, are shown in Fig. 10. The first mode, not shown in Fig. 10, is an in-plane mode with a frequency of 21.4 Hz. This mode does not change when the amount of pre-strain is changed as it only depends on the frame only.

Shown in Figs. 11-13 are the membrane deflection, RMS strain and LCO frequency versus flow velocity for the 5 percent pre-strain model at zero angle of attack. In both the experiment and theory, the first indication of instability occurs near 4.00 m/s and once again the trailing edge lower membrane membrane deflection slowly and smoothly increases with an increase in flow velocity. However, unlike the 2 percent pre-strain case, for 5 percent the computational model does not switch modes of vibration as the flow speed is changed. This mode of vibration, shown in Fig. 14 for flow at 8 m/s, is consistently one where the upper and lower membranes oscillate out-of-phase and appears to be a coupling between the third and fourth structural dynamic modes which are shown in Fig. 15.

As proposed above, the out-of-phase response of the membranes appears to explain the low level of strain seen in computational results in Fig. 12. On the other hand, the experimental meaurements show two levels of strain response, one low level which occurs from the onset of instability until approximately 6 m/s, and one high level which starts at 6 m/s. This switch in strain response corresponds to a switch in LCO frequency from one near 45 Hz. to a higher frequency near 52 Hz.

When this jump in frequency occurs in the experimental model it places the LCO frequency near that of the computation. However, while not shown here, a study of the experimental LCO mode of vibration for this case at the higher flow velocities after the jump occurs indicates an in-phase response of the membrane sections. This is consistent with the jump in strain response but not consistent with the mode of vibration noted in the computation which as previously stated is out-of-phase. This contradiction (approximately the same LCO frequency but different modes of vibration) perhaps points to the interesting possibility that there are two stable LCOs which can occur at a given flow velocity which differ mainly in mode of response. Depending on the initial conditions, which are unknown in the experiment, the solution could jump to either one of the two stable solutions. Future work will study the dependence of the LCO on initial conditions.

The final configuration for which detailed results are shown is the 7 percent pre-strain model. This level of pre-strain produces the only experimental results which demonstrate qualita-

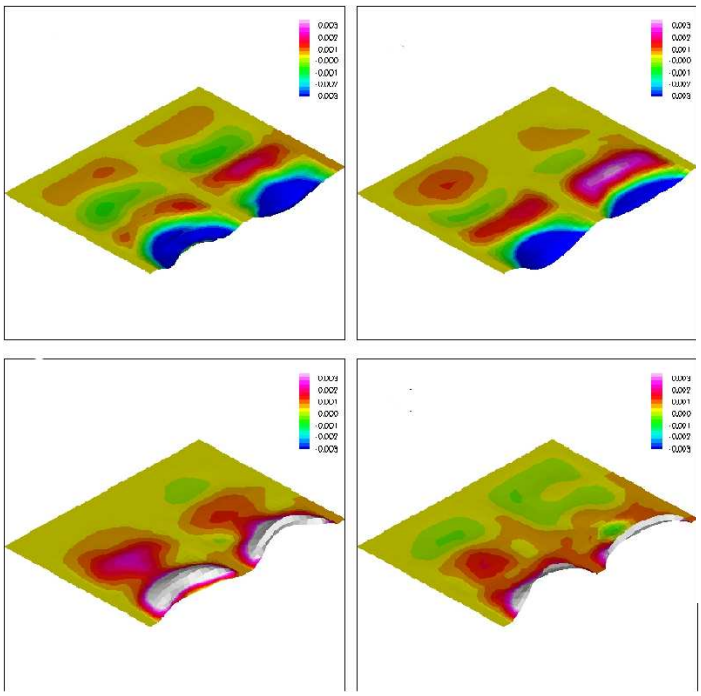

Figure 9. Computed spatial configuration (mode) of MMAV at 4 points in time during the limit cycle period for 2 percent pre-strain model at 0 degree angle of attack at 8.0 m/s

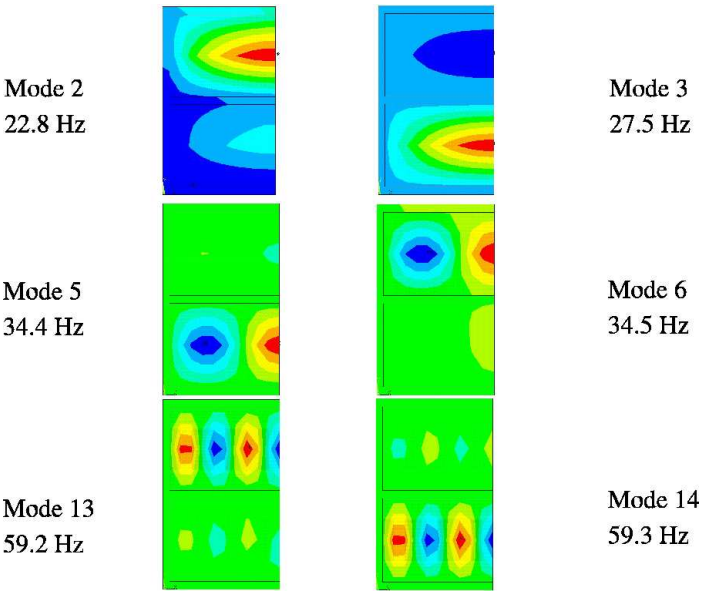

Figure 10. Contours of z deflection for structural modes of interest as generated with finite element modal analysis for the 2 percent pre-strain model.

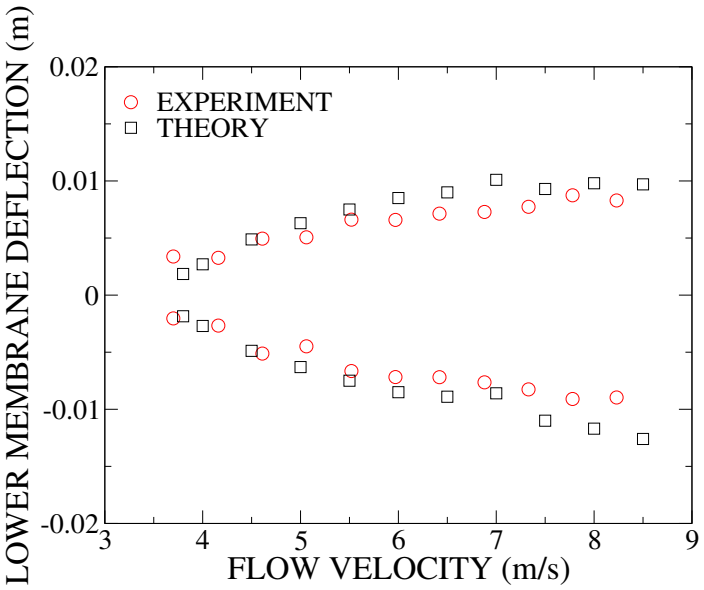

Figure 11. Deflection of MMAV versus flow velocity for 5 percent pre-strain model at 0 degree angle of attack.

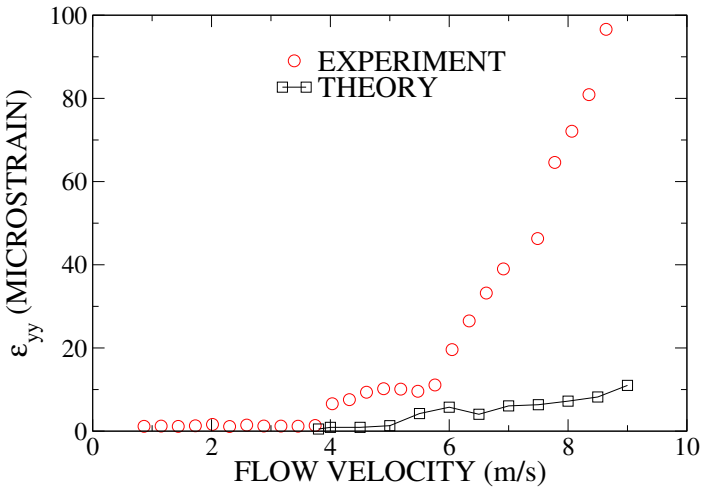

Figure 12. Root mean square of MMAV y normal strain versus flow velocity for 5 percent pre-strain model at 0 degree angle of attack.

tive differences when the static angle of attack is increased from 0 degrees. Shown in Figs. 16-18 are the membrane deflection, RMS strain and LCO frequency versus flow velocity for the 7 percent pre-strain model at zero angle of attack and 2 degree angle of attack (experiment only). At zero degree angle of attack the point of instability occurs near 4.40 m/s in the computation

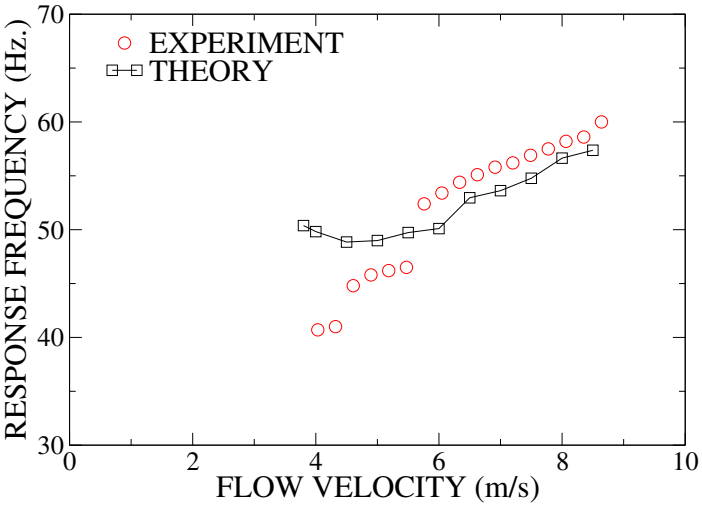

Figure 13. Dominant MMAV structural response frequency versus flow velocity for 5 percent pre-strain model at 0 degree angle of attack.

and 4.6 m/s in the experiment while for 2 degree angle of attack the experimental model shows onset of instability near 5.0 m/s.

While the 0 angle of attack computed flutter velocity (instability point) and membrane LCO amplitudes compare well with experiment, the frequency at which the LCO occurs does not. In the computation, the LCO frequency varies from 63.6 Hz. at 4.40 m/s to 62.3 Hz. at 7.00 m/s. The mode of vibration in the computation switches from in-phase when the flow velocity is equal to or below 4.50 m/s to out-of-phase when the velocity is increased to 5.00 m/s. This is shown in Fig. 19 which demonstrates the mode of response at the same point in the LCO period for flow velocities of 4.50 m/s and 5.00 m/s. Meanwhile the experimental LCO at 0 degree angle of attack occurs at a much higher frequency, starting off at 92.4 Hz at a flow velocity of 4.6 m/s and increasing smoothly to a maximum of 98.2 Hz. at a flow velocity of 8.35 m/s. There does appear to be a jump in frequency when the experiment is increased to 8.6 m/s at 0 degree angle of attack.

When the experimental strain and frequency data for 2 degrees is compared to the 0 angle of attack data, a substantial qualitative difference is observed. For 2 degrees, at the onset of the instability the frequency is 105.8 Hz. This increases to 106.5 Hz at 5.5 m/s before jumping to 92.3 Hz at 5.8 m/s. A final jump occurs between 7.8 m/s, where the dominant frequency of the LCO response is 95.1 Hz., and 8.1 m/s where the frequency is 128.2 Hz. These jumps in frequency correspond to the three different levels in strain response seen in Fig. 17.

As a conclusion to the discussion of the batten-reinforced fixed wing MMAV models, estimates for the flow velocity at which an LCO is first observed and the corresponding dominant LCO frequency are plotted versus percent pre-strain for 0 angle of attack in Figs. 20 and 21. As the pre-strain increases, both the

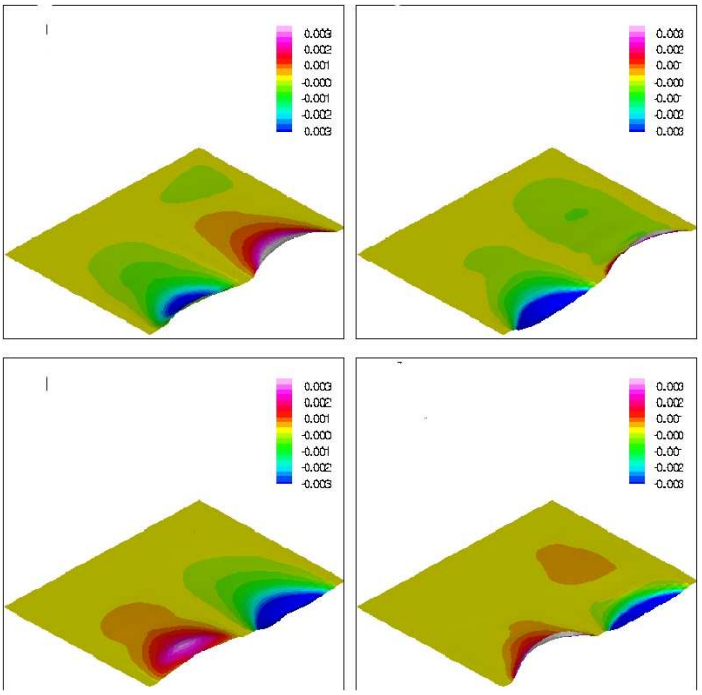

Figure 14. Computed spatial configuration (mode) of MMAV at 4 points in time during the limit cycle period for 5 percent pre-strain model at 0 degree angle of attack at 8.0 m/s

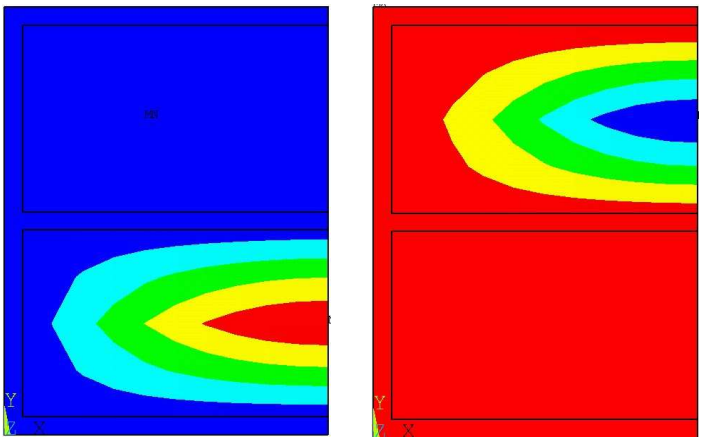

Figure 15. Contours of z deflection for structural modes of interest as generated with finite element modal analysis for the 5 percent pre-strain model.

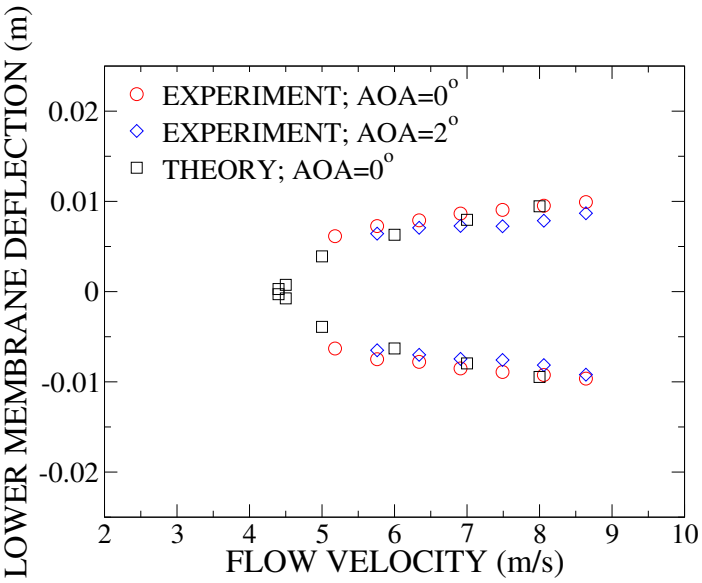

Figure 16. Deflection of MMAV versus flow velocity for 7 percent pre-strain model at 0 and 2 degree (experiment only) angle of attack.

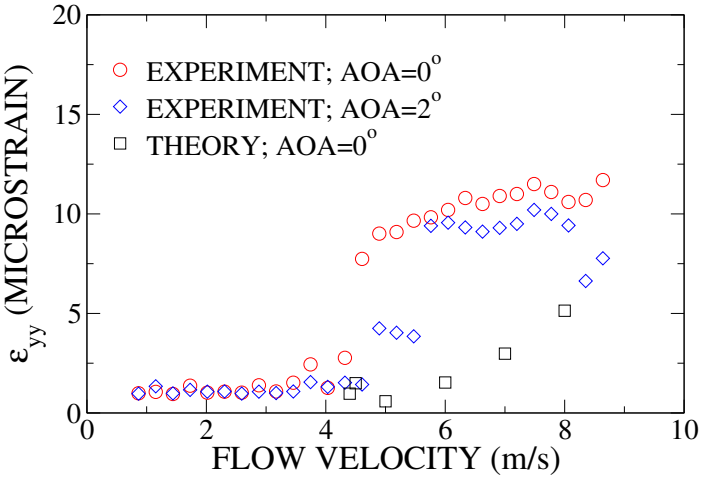

Figure 17. Root mean square of MMAV *y* normal strain versus flow velocity for 7 percent pre-strain model at 0 and 2 degree (experiment only) angle of attack.

LCO onset velocity and LCO frequency increase.

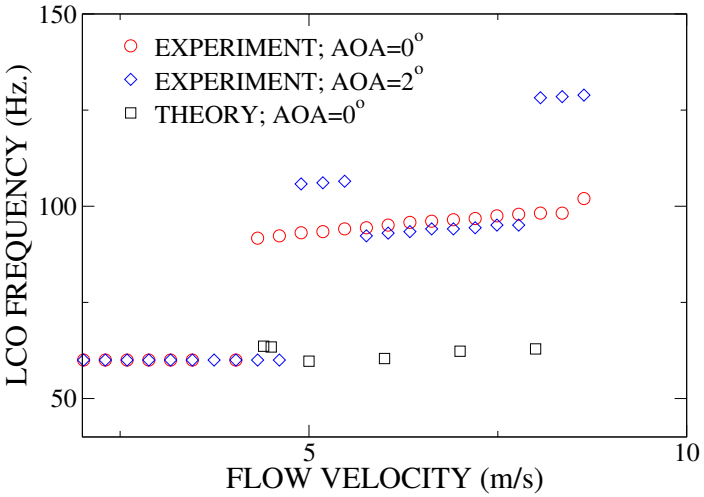

Figure 18. Dominant MMAV structural response frequency versus flow velocity for 7 percent pre-strain model at 0 and 2 degree (experiment only) angle of attack.

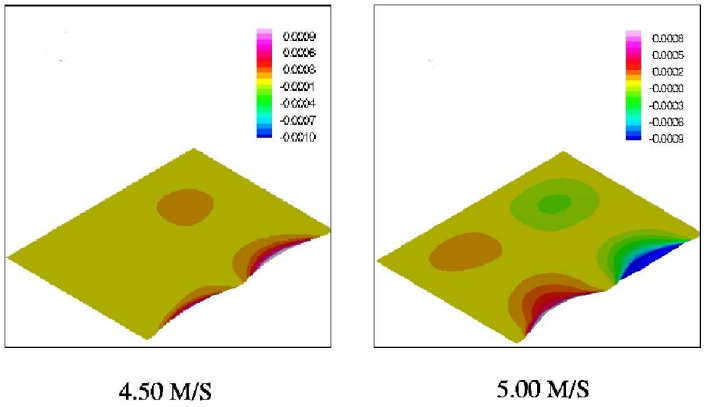

Figure 19. Computed spatial configuration (mode) of MMAV at 4 points in time during the limit cycle period for 7 percent pre-strain model at 0 degree angle of attack at 4.50 m/s and 5.00 m/s

Concluding Remarks

The configuration investigated consisted of a batten-reinforced fixed-wing MMAV constructed from an aluminum frame and latex material for the membrane. Experiments and computations were run for various levels of membrane pre-strain (2,5,7 and 10 percent) and fixed angle of attack (0 and 2 degrees reported here). For each configuration, a self-excited instability (flutter or Hopf bifurcation) occurred within the range of flow velocities examined. Overall, the agreement between the predicted and experimentally measured point of instability was good both

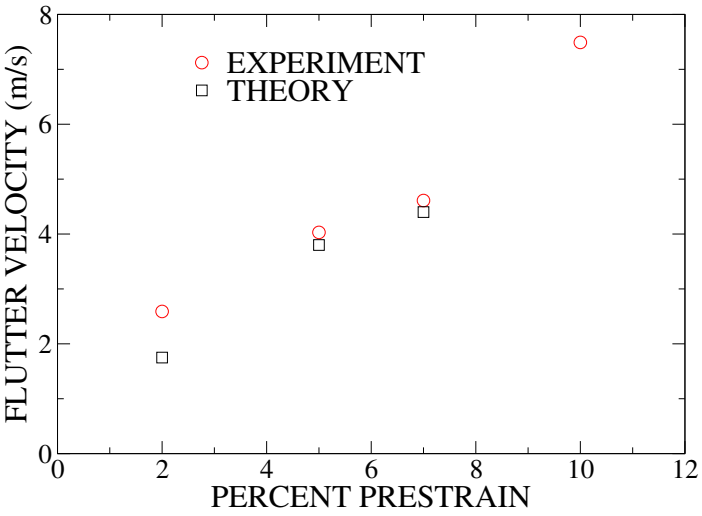

Figure 20. Limit cycle oscillation onset velocity versus level of membrane pre-strain for 0 degree angle of attack.

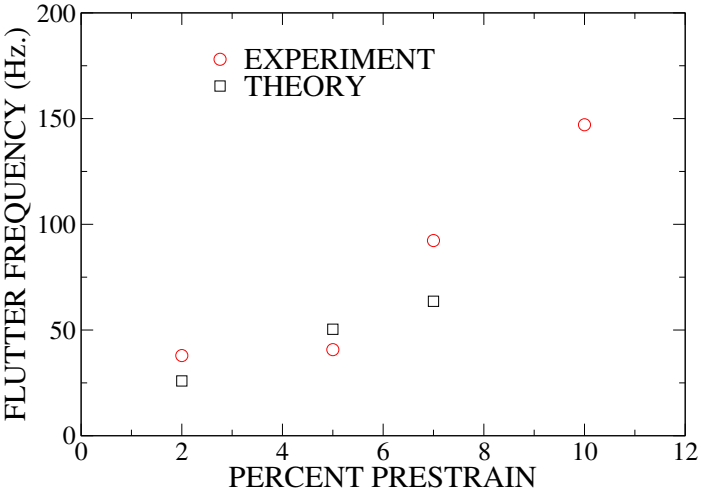

Figure 21. Limit cycle oscillation dominant frequency at onset velocity versus level of membrane pre-strain for 0 degree angle of attack.

showing an increase in the onset velocity and frequency with an increase in membrane pre-strain. Futhermore, both experiment and computation undergo a limit cycle oscillation (LCO) post-flutter and the agreement between the measured and predicted limit cycle amplitude at the trailing edge of the lower MMAV membrane is good.

A correlation between the mode of response and strain level is shown in the computation and postulated for the experiment. Computational results demonstrate that when the limit cycle oscillations occur with a mode of response which has both upper and lower membranes in-phase, a large amplitude strain response occurs at the measurement location (leading edge, near root). When this response is out-of-phase a drop in strain response is found.

Overall the computational and experimental agreement for the strain response and limit cycle oscillation frequency is fair but not as good as the prediction of the flutter point and trailing edge membrane LCO amplitude. This would perhaps indicate that , for some cases, the computation and experiment exhibit different modes of oscillation. An example of this differing behavior is the behavior of the LCO frequency as the flow velocity is increased beyond that of the initial instability velocity. Both the experiment and computational models show a change in the dominant limit cycle frequency with a change in flow velocity. However the computational model change is smooth while for many of the cases tested the experiment appears to exhibit discrete jumps in frequency indicating a dramatic change in oscillation mode. These jumps are most often correlated with jumps in the strain response perhaps indicating changes in the phase of the upper and lower membrane deflection. The computational aerodynamic model does not include viscous effects, hence it is possible that discrepancies in the limit cycle oscillation frequencies could be due to the neglect of viscosity. It is possible that flow separation and vortex shedding could be occuring after the onset of flutter which could have an effect on the the characteristic limit cycle response.

Both computation and experiment aeroelastic response exhibit almost no sensitivity to the static angle of attack for the cases investigated. The exception to this is the experimental model with 7 percent pre-strain. For this case, significant differences in the strain response and LCO frequency exist between the zero and two degree angle of attack cases. At zero angle of attack, both the strain response and LCO frequency vary smoothly with flow velocity while these measurements display significant jumps at two flow velocities for the model at two degree angle of attack. The LCO frequency at the onset of the limit cycle response also differs significantly (92.4 Hz. for 0 degrees versus 105.8 Hz. for 2 degrees).

Acknowledgements

The first author would like to acknowledge the support of the American Society for Engineering Education (ASEE) which provided a summer faculty fellowhip to fund this work. The first author would also like to acknowledge The University of Oklahoma Research Council which provided funding for the construction of the experimental model investigated in this paper. Finally, the authors would also like to acknowledge The University of Oklahoma Supercomputing Center(OSCER) which provided supercomputing time to the authors enabling them to complete this work.

REFERENCES

[1] Heathcote, S., Wang, Z., and Gursul, I., 2008. "Effect of spanwise flexibility on flapping wing propulsion". *Journal of Fluids and Structures,* **24**, pp. 183–199.

[2] Heathcote, S., and Gursul, I., 2007. "Flexible flapping airfoil propulsion". *AIAA Journal,* **45**(5), May, pp. 1066–1079.

[3] Lian, Y., Shyy, W., Viieru, D., and Zhang, B., 2003. "Membrane wing aerodynamics for micro air vehicles". *Progress in Aerospace Sciences,* **39**, pp. 425–465.

[4] Shyy, W., Ifju, P., and Viieru, D., 2005. "Membrane wing-based micro air vehicles". *Applied Mechanics Reviews,* **58**, pp. 283–301.

[5] Lian, Y., and Shyy, W. Three-dimensional fluid-structure interactions of a membrane wing. AIAA Paper 2003-1726.

[6] Lian, Y., and Shyy, W., 2007. "Laminar-turbulent transition of a low reynolds number rigid or flexible airfoil". *AIAA Journal,* **45**(7), July.

[7] Lian, Y., and Shyy, W., 2007. "Numerical simulations of membrane wing aerodynamics for micro air vehicle applications". *Journal of Aircraft,* **42**(4), pp. 865–873.

[8] Waszak, R., Jenkins, N., and Ifju, P. Stability and control properties of an aeroelastic fixed wing micro aerial vehicle. AIAA Paper 2001-4005, Presented at the AIAA Atmospheric Flight Mechanics Conference, Montreal, Canada, August 6-9, 2001.

[9] Hu, H., Tamai, M., and Murphy, J. T., 2008. "Flexible-membrane airfoils at low reynolds numbers". *Journal of Aircraft,* **45**(5), September-October, pp. 1767–1778.

[10] Johnston, J. W., Romberg, W., Attar, P. J., and Parthasarathy, R., 2010. "Experimental characterization of limit cycle oscillations in membrane wing micro air vehicles". *Journal of Aircraft*. Accepted.DOI:10.2514/1.47258.

[11] Mann, P., 2004. *Introductory Statistics*, 5th ed. Wiley, New York.

[12] Attar, P. J., 2007. "Some results for an approximate rotation tensor formulation in geometrically nonlinear Reissner-Mindlin plate theory". *International Journal for Non-Linear Mechanics*. doi:10.1016/j.ijnonlinmec.2007.10.006.

[13] Katz, J., and Plotkin, A., 2001. *Low-Speed Aerodynamics*, second ed. University Press, Cambridge.

[14] Attar, P., and Gordnier, R. Aeroelastic modeling using a geometrically nonlinear p-version mixed reissner-mindlin plate element. AIAA Paper 2007-2318 Presented at the 48th AIAA Structures,Structural Dynamics and Materials Conference, Honolulu, HI, April 23-26 2006.

[15] ANSYS INC., 2008. *ANSYS User Manual, Release 11.0*.